Nano Lett., volume 16, pages 1884–1889, year 2016 // Dynamics of Spatially Confined Bisphenol A Trimers in a Unimolecular Network on Ag(111)

Julian A. Lloyd,[1] Anthoula C. Papageorgiou,[1, a)] Sybille Fischer,[1] Seung Cheol Oh,[1] Özge Sağlam,[1] Katharina Diller,[1, 2] David A. Duncan,[1] Francesco Allegretti,[1] Florian Klappenberger,[1] Martin Stöhr,[2] Reinhard J. Maurer,[2] Karsten Reuter,[2] Joachim Reichert,[1, b)] and Johannes V. Barth[1]

[1)] *Physik Department E20, Technische Universität München, 85748 Garching, Germany*

[2)] *Theoretische Chemie, Technische Universität München, 85748 Garching, Germany*

Bisphenol A (BPA) aggregates on Ag(111) shows a polymorphism between two supramolecular motifs leading to formation of distinct networks depending on thermal energy. With rising temperature a dimeric pairing scheme reversibly converts into a trimeric motif, which forms a hexagonal superstructure with complex dynamic characteristics. The trimeric arrangements notably organize spontaneously into a self-assembled one-component array with supramolecular BPA rotors embedded in a two-dimensional stator sublattice. By varying the temperature, the speed of the rotors can be controlled as monitored by direct visualization. A combination of scanning tunneling microscopy and dispersion-corrected density-functional tight-binding (DFTB-vdW$^{\mathrm{surf}}$) based molecular modeling reveals the exact atomistic position of each molecule within the assembly as well as the driving force for the formation of the supramolecular rotors.

Keywords: Self-assembly, rotor arrays, scanning tunneling microscopy, dispersion-corrected density-functional tight-binding, silver surface

During the past decade, molecular rotors and motors on interfaces have been the central topic of numerous investigations.[1−8] While many of the studies focus on isolated single rotors on well-defined surfaces, it is mandatory for potential applications, such as novel sensors and signal processing,[9] to have the ability to tailor entire arrays of molecular rotors. Different approaches have been used to achieve this goal, including the use of bimetallic dislocation networks to provide regular adsorption sites for molecular rotors[10,11] or the formation of molecular networks confining the rotors within their cavities.[1−3,12−14] In our study we present a single-component system solely built with bisphenol A molecules, showing different temperature-dependent supramolecular assemblies and intriguing dynamic behavior on a Ag(111) surface. We notably find a regular hexagonal structure containing mobile supramolecules, whose rotational speed could be controlled by the temperature.

Bisphenol A (BPA, systematic name: 4,4′-(propane-2,2-diyl)diphenol, Figure 1) is commonly used as a chemical in polymerization reactions for household plastics and is suspected to have hazardous effects as an endocrine disruptor.[15−17] The experiments presented in this study address the self-assembly of the BPA on an Ag(111) surface which is governed by a particularly subtle interplay of molecule–molecule and molecule–substrate interactions. A previous combined scanning tunneling microscopy (STM), X-ray photoelectron spectroscopy (XPS), and near edge X-ray absorption fine structure (NEXAFS) study on the close-packed Cu(111) surface revealed a rich set of temperature-dependent structural transitions caused by a stepwise deprotonation of the BPAs hydroxyl groups.[18] The related noble-metal Ag(111) surface used in the work presented herein provides an assembly platform where lateral molecule–molecule interactions are expected to prevail.

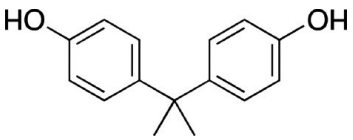

FIG. 1. Structure of bisphenol A (BPA).

Our STM investigations of BPA on Ag(111) reveal the formation of three different, partially coexisting regular two-dimensional structures that display a strong temperature dependence. In the range between 180 and 250 K, two different networks composed of molecular dimers exist on the surface (Figure 2), whereas at sample temperatures between 250 and 340 K an additional third phase (Figure 3) evolves consisting of hexagonally arranged trimeric units. This phase coexists with the dimeric phases, but for temperatures exceeding 300 K represents the prevailing arrangement. The formation of the trimeric phase is reversible; i.e., upon cooling the sample to temperatures below 250 K it dissolves, leaving only the dimeric structures on the surface. XPS suggests a slight degree of deprotonation of the hydroxyl groups starting just below room temperature, but this does not affect the reversibility of the transition (Supporting Information, Figure S1). After heating to 340 K the binding energy of the 1s peaks of both oxygen and carbon do not shift further in energy when probed at different tempera-

[a)] Electronic mail: a.c.papageorgiou@tum.de
[b)] Electronic mail: joachim.reichert@tum.de

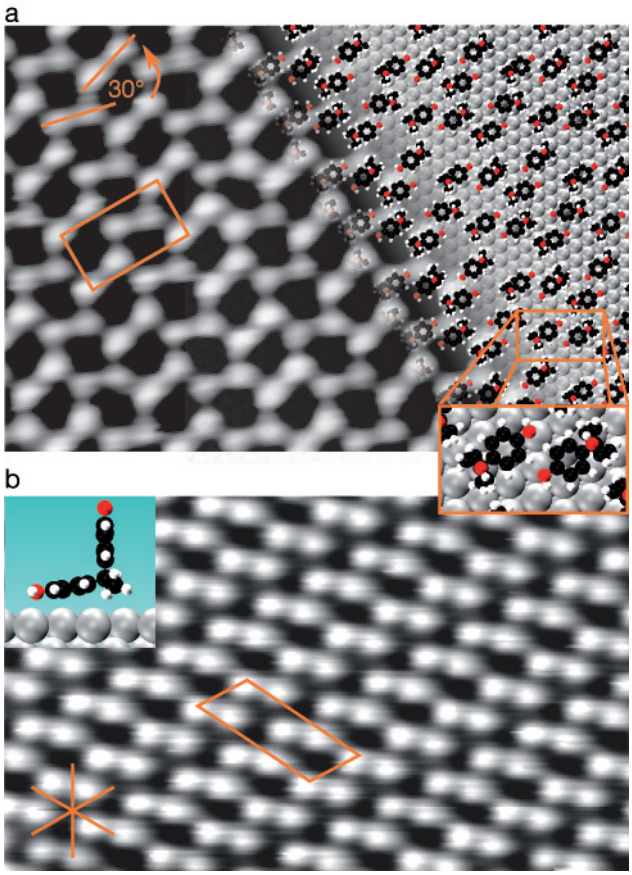

FIG. 2. STM images and molecular models of the two different dimeric structures of BPA on Ag(111) in the 180 − 250 K regime. (a) STM image of the arrangement consisting of dimers with two different orientations (tilted dimer arrangement, 12.9×8.8 nm^2, $U_{\mathrm{bias}} = 1.25$ V, $I = 0.13$ nA, $T = 190$ K). Right part superposed with simulated geometry. The unit cell and the dimers orientations are indicated in orange. Inset: Magnification of the paired BPA unit indicated in the model. (b) STM image of the dimeric assembly comprising dimers with identical orientations and an oblique unit cell indicated in orange (staggered dimer arrangement, 13.3×8.0 nm^2, $U_{\mathrm{bias}} = 1.25$ V, $I = 0.12$ nA, $T = 190$ K). Inset at upper left: Side view of a BPA molecule on the surface. The substrates high symmetry axes are marked in orange.

tures. For all molecular models shown below the BPA is assumed to be in its intact form. Annealing above 340 K results in desorption of the molecules.

The identified dimeric structures comprise both the same molecular dimer units with a center-to-center distance of 7.5 ± 0.7 Å, which are tilted by $15 \pm 0.5°$ with respect to the substrate's $< 1\bar{1}0 >$ directions, resulting in six different surface orientations. Specifically, the first superlattice consists of dimers with different orientations, forming an angle of $30 \pm 0.5°$ between them ("tilted dimeric arrangement", Figure 2a). The resulting rectangular unit cell has side lengths of 23 ± 1 Å (running along the high symmetry axis) and 13 ± 1 Å. The second assembly is more densely packed and consists of dimers, which are all aligned in the same direction in a staggered arrangement. It is characterized by an oblique unit cell with sides of 26 ± 1 Å and 12 ± 1 Å, both running along the Ag(111) high symmetry directions (cf. Figure 2b).

NEXAFS reveals an average tilt angle of $40° \pm 10°$ for the phenol rings with respect to the surface plane (see Supporting Information, Figure S2), which leaves two plausible orientations for the molecules. One option is an "L-shaped" conformation of the molecule where one phenol ring aligns almost parallel ($\sim 10°$) to the silver surface and the other phenol ring pointing out of the surface with a tilt angle of $70 - 80°$ with respect to the substrate (Supporting Information, Figure S3a,b). The second option is a circumflex-shaped conformation of the two phenol rings with both rings being tilted by $30 - 40°$ with respect to the surface and both hydroxyl groups pointing toward it (Supporting Information, Figure S3c,d). Since it is not possible to reconcile the observed densely packed dimer structure with the more expansive circumflexed configuration of the molecules, the combined experimental evidence suggests the dimers in Figure 2 to be built by molecules featuring the "L-shaped" configuration. To substantiate this hypothesis and obtain more insight into the molecular ordering and relative stability of the observed networks, we additionally employed dispersion-corrected density-functional tight-binding (DFTB-vdW$^{\mathrm{surf}}$) based molecular modeling. Taking into consideration the packing density revealed by STM for the tilted dimer arrangement, the unit cell for the modeling consisted of four BPA dimers in a rhombic Ag(111) surface slab (cf. Supporting Information, Figure S4). The structure models shown in the insets of Figure 2 are the result of the geometry optimization of these dimer structures on the Ag(111) surface (see Supporting Information for additional details). The derived molecular conformation (inset in Figure 2b) agrees well with the experimentally inferred "L-shape" of the BPA dimers. The flat-lying phenol rings point toward each other, allowing attractive interactions between the phenol ring and the opposing hydroxyl group[19] (cf. inset in Figure 2). Furthermore, this configuration allows for dispersive interactions of the aromatic phenyl ring with the underlying surface. In addition, excellent agreement can be found between the tilted arrangement of dimers imaged by STM (in Figure 2a) and the corresponding overlaid simulated structure (top right corner of Figure 2a and S4).

Increasing the sample temperature in the range between 250 and 340 K results in the emergence of a third structure, now comprising trimeric units. Here, six trimers (marked by green triangles in Figure 3c) form a hexagonal cavity with additional molecules trapped inside (marked by the orange circle in Figure 3c). At room temperature the latter appear fuzzy, indicating a high mobility of the caged entities constrained by the trimers forming the cavity. The diameter of the dynamic unit was determined to be approximately 12 ± 2 Å. It has an organizational chirality expressed by the orientation of

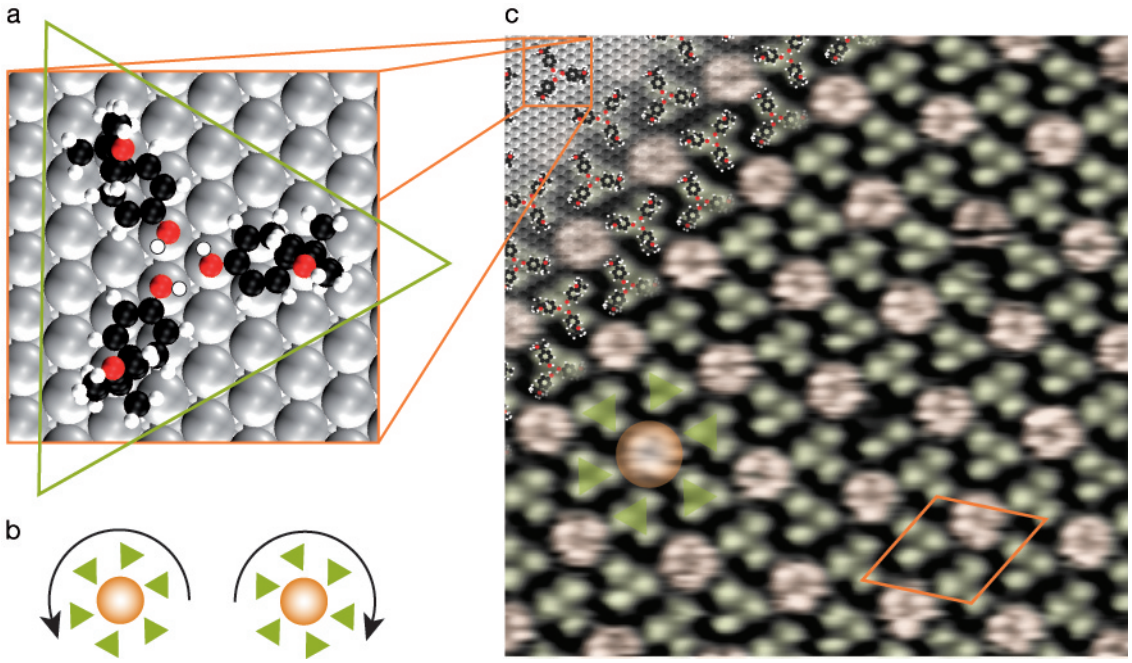

FIG. 3. Trimeric network at room temperature. (a) Top view of the geometry optimization of a BPA trimer on the Ag(111) surface, whose sides align with the high symmetry axes of the Ag(111) substrate as indicated by the green triangle. (b) Schematic representation of both enantiomers of the motif with the trimers represented by green triangles and the mobile center by an orange circle. (c) STM image of the trimeric motif recorded at room temperature (16.7×16.6 nm^2, $U_{\mathrm{bias}} = 1.25$ V, $I = 0.12$ nA) with superimposed atomistic model of the stationary trimers (top left corner). The hexagonal unit cell of the trimeric assembly is indicated in orange.

the single trimers with respect to the center. The respective enantiomeric motifs are schematically illustrated in Figure 3b. Both enantiomers were observed in the STM data (see also Figure S5), but individual domains were homochiral. The hexagonal unit cell has a side length of 30 ± 1 Å where the axes of the unit cell are rotated by $\sim 20°$ with respect to the silver $< 1\bar{1}0 >$ directions. The static trimers are characterized by an intermolecular spacing of 8.0 ± 1 Å. The average phenol orientation of this phase was also studied by NEXAFS measurements, which revealed the same variation of intensities of the π^* adsorption features as a function of the angle of photon incidence at both 190 and 300 K (Supporting Information, Figure S2b).

In a temperature range of approximately 250–260 K, some trapped species are transiently immobilized on a time scale that can be resolved by the STM and can be identified to consist of BPA trimers (highlighted in orange in Figure 4a) as well. When visible, the inner trimers are always orientated with three of their lobes facing the three neighboring trimers, while keeping the inner trimeric distances constant. Upon annealing slightly above 260 K, a complete mobilization of the inner species sets in (at least on time scales that can be resolved by STM) and at no point could all mobile trimers be frozen out as cooling below 250 K resulted in a phase transition to dimeric structures (as discussed above).

As images with coexisting dimer and trimer structures did not show any difference in the appearance of the protrusions (Supporting Information, Figure S5), we propose the same molecular orientation for the BPA within the trimer motif (Figure 3) as for the dimer. In this model, the trimer itself (whether rotor or static) would be stabilized by cyclic hydrogen bonds between the hydroxyl groups,[20] whereas the edges of the whole static trimer motif align with the underlying Ag(111) surface, outlined in green in Figure 3a.

The STM images also distinguish two metastable states (marked in orange and blue coloring in Figure 4c,d,f,g) for the caged trimers with transitions between them. As the mobile trimers have 3-fold symmetry, each metastable position corresponds to three orientations of the trimer, adding up to six orientations between which the trimer can switch by rotational motion (see inset Figure 5). Accordingly the mobile trimer can be considered as a rotor with a metastable position every 60°. In order to investigate the thermal behavior of the rotor, images taken at different temperatures were analyzed. The mobility of different trimers at the same sample temperature varies substantially (see Figure 4), bedeviling a systematic analysis of the dynamics. The differences are presumably caused by the slight amount of deprotonated species observed by XPS. Nevertheless, general trends of temperature dependence could still be observed (see Figure S6 for more information on the rotor dynamics). The rates increase significantly when increasing the

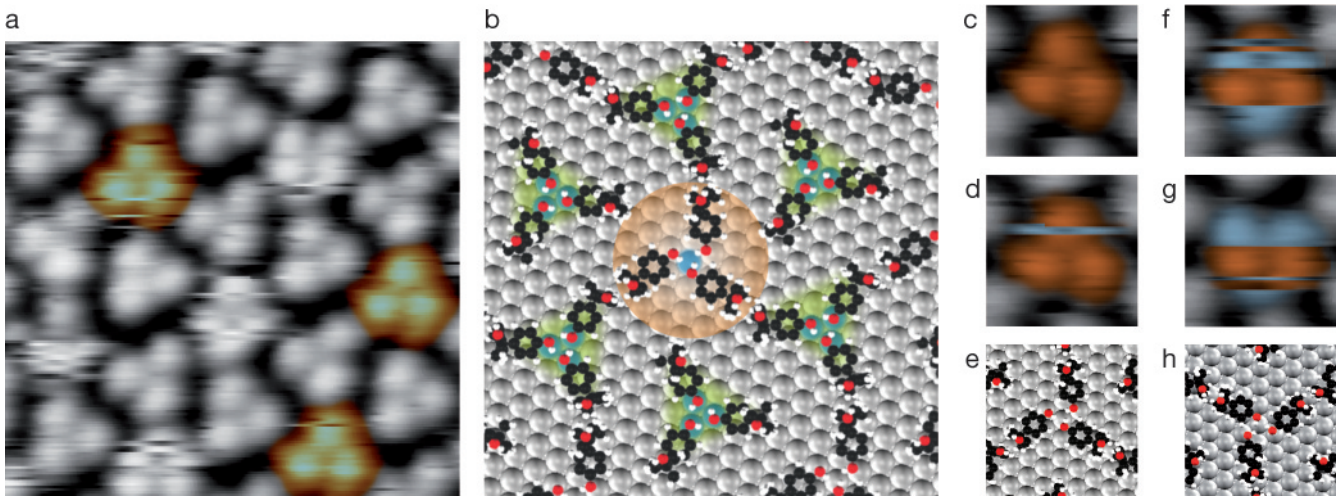

FIG. 4. Mobility of the trapped trimers: (a) Immobilized caged trimers (colored) coexisting with rotating caged trimers (8.6×8.6 nm^2, $U_{\text{bias}} = 1.25$ V, $I = 0.13$ nA, $T = 255$ K). (b) DFTB + vdW$^{\text{surf}}$ optimized trimer structure. The static trimers (highlighted in green) cage an immobilized trimer (highlighted in orange). The adsorption sites of the centers of the trimer motifs are indicated by coloring blue the underlying Ag atoms. (c,d,f,g) Different trimers at the same temperature ($U_{\text{bias}} = 1.25$ V, $I = 0.13$ nA, $T = 255$ K, side length: 2 nm). The blue and orange colored protrusions indicate the two inequivalent metastable positions of the trimers. Switching occurs several times during scanning of the trimers (Image acquisition time: 1.4 s). (e,h) Molecular structures of the two distinguishable positions of the immobilized trimers found to be metastable in the DFTB + vdW$^{\text{surf}}$ simulation.

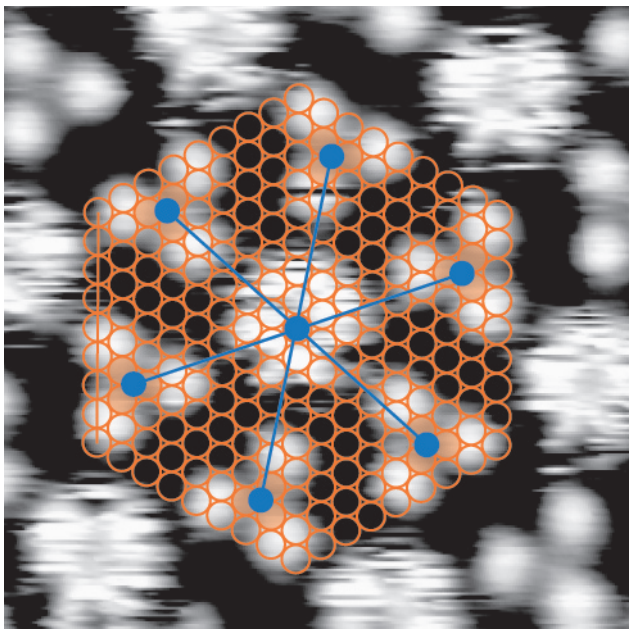

FIG. 5. STM image of a single hexagon (6.2×6.2 nm^2, $U_{\text{bias}} = 1.49$ V, $I = 0.11$ nA, $T = 290$ K) with superimposed atomic lattice of the underlying Ag(111) surface. The centers of the trimers are marked in blue to compare their adsorption sites. The inset illustrates the rotary motion of the central trimer.

temperature and different metastable states were quickly indistinguishable (Figure 3c).

For the etiology of the remarkable mobility differences of the BPA trimers within the structure, a careful analysis of the geometry of the arrangement was performed. The hexagonal symmetry of the structure as well as the relatively large distances between individual trimers, together with the existence of the rotating trimers, might indicate that the static trimers are stabilized by interaction with the surface, e.g., as a result of preferred adsorption sites, rather than by interactions between neighboring trimers. This idea can be supported by overlaying the atomic lattice of the Ag(111) surface on top of the STM image (Figure 5) with the centers of the static trimers and the mobile species indicated in blue. Positioning the lattice in such a way that the centers of the static trimers are at equivalent lattice points, results in only a single possible configuration within the uncertainty of our STM image calibration, which is presented in Figure 5. This configuration positions the centers of the static trimers on either hcp or fcc hollow sites (depending on the orientation of the trimers; pointing left or right in Figure 5) resulting in equivalent adsorption sites for all molecules within all static trimers. Remarkably, with this configuration, the center of the hexagon formed by the static trimers (i.e., the center of the rotor), lies on an atop site of the Ag(111) surface rather than on a hollow site as inferred for the static trimers (Figure 5) (see Figure S7 for a tentative molecular model of the whole arrangement). Preventing a molecule from occupying its favored adsorption site, that is, moving it out of registry, has been shown to lower the energy barrier for rotational and similarly translational movements significantly.[21,22]

As done before for the dimeric units, we modeled by DFTB + vdW$^{\text{surf}}$ the trimeric structure to obtain information about the conformational details and stability. In

a first step only the static trimers were considered by optimizing two BPA trimers in a corresponding hexagonal unit cell (cf. Figures 3a and S8). The lowest energy configuration was found for trimers placed on hollow positions where each oxygen atom adsorbs slightly offset from an *atop* position as known for other oxygen linked adsorbates, e.g., ethanol or water on Ag(111).[20] In addition to this preferred positioning of the oxygen atoms, the cyclic arrangement of the hydroxyl moieties forming the center of the trimer unit allows hydrogen bonding[23] between the three BPA molecules around a *hollow* site (cf. Figure 3a). To describe the rotor, a third trimer was placed in the same unit cell (cf. Figures 4b and S8) at different starting positions with respect to the first two trimers, resulting in several different metastable configurations for the caged trimer. For all optimized models, the hexagonal array of six trimers adsorbed around hollow sites remained stable, whereas the position and stability of the central trimer varied to a great extent. This is not surprising, given that for the caged trimer the availability of possible adsorption sites is limited by lateral repulsion from the static trimers. Depending on the initial orientation of the caged trimer with respect to the stators, both metastable and unstable central trimer configurations were found (examples are shown in Figure 3e,h and S8). We note that ground state energy differences between the different metastable caged trimer structures are small (1–5 meV per BPA molecule), which is in line with the experimental observation of thermal averaging between several metastable configurations. Experimentally we observed that the rotor can be temporally immobilized (Figure 4) in the metastable configurations, as shown in Figure 4e,h. Therefore, it is proposed that the caged trimer consists of a rotor which transits between six metastable configurations, resulting in only two symmetrically inequivalent positions of the caged trimer (highlighted in blue and orange in Figure 4). The adsorption energies per BPA molecule were similar for all optimized trimer phases (Figures S8–9), but lower than those observed for the dimer phases (Figure S4) (2.04 eV/BPA vs 2.18 eV/BPA). Along with the decrease of packing density (0.013 BPA per Å^2 for dimeric phases to 0.010 BPA per Å^2 for the trimeric) this points to a gain in entropy as the driving force for the phase transition between dimeric and trimeric phases at higher temperatures.

Thus, by carefully analyzing STM images as well as by DFTB + vdW$^{\text{surf}}$ simulations, we attribute the instability of the trapped trimer, resulting in its rotational motion, to an unfavorable adsorption position to which the trimer is steered by the surrounding molecular arrangements. The entailed different adsorption site of the rotors compared to the static trimers is nicely confirmed by the higher apparent height of the mobile species, when frozen out (Figure S10).

Summary.

We investigated BPA with a combination of complementary surface and nanoscale science tools on the Ag(111) surface. We observed a polymorphism of dimeric arrangements and a trimeric structure whereby the trimeric motif vanishes below 250 K. Molecular models for both the dimer and the trimer motifs were presented based on experimental evidence (STM, NEXAFS) and theoretical calculations (DFTB + vdW$^{\text{surf}}$).

The trimeric phase shows a periodic array of mobile supramolecules caged in a grid of hexagonally arranged trimer units. Remarkably, the mobile species could also be identified as trimers. Therefore, a system of supramolecular rotors, which are confined by a matrix of the same kind of supramolecules on an only weakly corrugated surface, was observed. The switching between six metastable positions of the trimers by a rotational movement on the Ag(111) surface was attributed to an induced instability caused by the mobile trimer being forced, by the matrix of its local environment, into a nonideal adsorption site. The pertaining surface architecture consists of extended, almost defect-free arrays of supramolecular rotors on the surface, offering new pathways to tailor functionalized surfaces with numerous potential applications, such as novel sensors and signal processing.

Methods.

Sample Preparation. The atomically flat Ag(111) single crystal surface was prepared in UHV by repeated cycles of Ar^+ sputtering and annealing at 630 K. The BPA molecules (Sigma-Aldrich, purity > 99%) were outgassed in vacuo at the temperature close to their sublimation point and subsequently sublimed in situ onto the surface from a quartz crucible at $\sim$ 390 K with the sample held at room temperature (STM measurements) or at $\sim$ 120 K (synchrotron measurements).

STM Measurements. A variable temperature STM (Specs, "Aarhus 150"), mounted in a custom designed UHV chamber (base pressure $\sim 4\times10^{-10}$ mbar) was utilized for the STM measurements. These measurements were carried out at sample temperatures between 150 and 330 K with the etched W tip held at room-temperature. U_{bias} is the tunneling bias applied to the sample. The sample temperature was changed during scanning, which enabled the in situ observation of temperature induced changes. Additionally, an extensive series of annealing steps at different temperatures was carried out, and the sample was scanned after each step at a defined temperature. STM data were processed using the WSxM software.[24]

XPS and NEXAFS Synchrotron Measurements. XPS and NEXAFS measurements were carried out at the HE-SGM dipole beamline at the BESSY II storage ring in Berlin. The relevant experimental details can be found

in the Supporting Information.

DFTB + vdW^{surf} Based Molecular Modeling. Simulations were performed using the DFTB code DFTB+ (version 1.2.2)[25] in combination with the Atomic Simulation Environment.[26] Herefore an optimized set of parameters was generated using the code Hotbit.[27,28] A pairwise additive dispersion-correction (vdW^{surf}) that is specifically designed to accurately describe the interaction of large organic adsorbates with metal substrates was added.[29,30] The BPA molecules were placed on six-layered Ag(111) surface slabs with a lattice constant of $\alpha = 4.14$ Å, where the two topmost layers were explicitly treated within the DFTB framework. All six layers were described using vdW^{surf}, which allows the optimization of the here presented large unit cells with up to nine BPA units. Additional settings and details on the DFTB + vdW^{surf} approach can be found in the Supporting Information.

ACKNOWLEDGMENTS

This work was enabled by the ERC Advanced Grant MolArt (No. 247299). A.C.P., Ö.S., and D.A.D. were supported by a Marie Curie Intra-European Fellowship (project NASUMECA, No. 274842), a Marie Curie International Incoming Fellowship (Project NANOULOP, No. 302157), and the Alexander von Humboldt Foundation, respectively. We thank Helmholtz-Zentrum Berlin (HZB) for the allocation of synchrotron radiation beamtime and financial support. Dr. A. Nefedov and Prof. Ch. Wöll are gratefully acknowledged for providing access to the HE-SGM end station.

ASSOCIATED CONTENT

The Supporting Information is available free of charge on the ACS Publications website at DOI: 10.1021/acs.nanolett. 5b05026.

O 1s core level; NEXAFS C K-edge spectra and curve fitting analysis; plausible adsorption modes of BPA on Ag(111); STM images of a coexisting dimer and trimer phases; Menzel-Schlichting plot of the rotor dynamics; molecular model of trimer phase; STM apparent height of immobilized and static trimers; experimental details for XPS and NEXAFS; computational details and additional results of the tight-binding based molecular modeling

REFERENCES

1. Schull, G.; Douillard, L.; Fiorini-Debuisschert, C.; Charra, F.; Mathevet, F.; Kreher, D.; Attias, A.-J. *Nano Lett.* **2006**, *6*, 1360.

2. Wintjes, N.; Bonifazi, D.; Cheng, F.; Kiebele, A.; Stöhr, M.; Jung, T.; Spillmann, H.; Diederich, F. *Angew. Chem., Int. Ed.* **2007**, *46*, 4089.

3. Wahl, M.; Stöhr, M.; Spillmann, H.; Jung, T. A.; Gade, L. H. *Chem. Commun.* **2007**, 1349.

4. Michl, J.; Sykes, E. C. H. *ACS Nano* **2009**, *3*, 1042.

5. Balzani, V.; Credi, A.; Venturi, M. *ChemPhysChem* **2008**, *9*, 202.

6. Browne, W. R.; Feringa, B. L. *Nat. Nanotechnol.* **2006**, *1*, 25.

7. Hla, S.-W. *Nat. Nanotechnol.* **2007**, *2*, 82.

8. Écija, D.; Auwärter, W.; Vijayaraghavan, S.; Seufert, K.; Bischoff, F.; Tashiro, K.; Barth, J. V. *Angew. Chem., Int. Ed.* **2011**, *50*, 3872.

9. de Jonge, J. J.; Ratner, M. A.; de Leeuw, S. W.; Simonis, R. O. *J. Phys. Chem. B* **2004**, *108*, 2666.

10. Bellisario, D. O.; Baber, A. E.; Tierney, H. L.; Sykes, E. C. H. *J. Phys. Chem. C* **2009**, *113*, 5895.

11. Gao, L.; Liu, Q.; Zhang, Y. Y.; Jiang, N.; Zhang, H. G.; Cheng, Z. H.; Qiu, W. F.; Du, S. X.; Liu, Y. Q.; Hofer, W. A.; Gao, H. J. *Phys. Rev. Lett.* **2008**, *101*, 197209.

12. Kühne, D.; Klappenberger, F.; Krenner, W.; Klyatskaya, S.; Ruben, M.; Barth, J. V. *Proc. Natl. Acad. Sci. U. S. A.* **2010**, *107*, 21332.

13. Palma, C.-A.; Björk, J.; Rao, F.; Kühne, D.; Klappenberger, F.; Barth, J. V. *Nano Lett.* **2014**, *14*, 4461.

14. Palma, C.-A.; Björk, J.; Klappenberger, F.; Arras, E.; Kühne, D.; Stafström, S.; Barth, J. V. *Nat. Commun.* **2015**, *6*.

15. Tharp, A. P.; Maffini, M. V.; Hunt, P. A.; VandeVoort, C. A.; Sonnenschein, C.; Soto, A. M. *Proc. Natl. Acad. Sci. U. S. A.* **2012**, *109*, 8190.

16. Bromer, J. G.; Zhou, Y.; Taylor, M. B.; Doherty, L.; Taylor, H. S. *FASEB J.* **2010**, *24*, 2273.

17. Doshi, T.; Mehta, S. S.; Dighe, V.; Balasinor, N.; Vanage, G. *Toxicology* **2011**, *289*, 74.

18. Fischer, S.; Papageorgiou, A. C.; Lloyd, J. A.; Oh, S. C.; Diller, K.; Allegretti, F.; Klappenberger, F.; Seitsonen, A. P.; Reichert, J.; Barth, J. V. *ACS Nano* **2014**, *8*, 207.

19. Arras, E.; Seitsonen, A. P.; Klappenberger, F.; Barth, J. V. *Phys. Chem. Chem. Phys.* **2012**, *14*, 15995.

20. Tereshchuk, P.; Da Silva, J. L. F. *J. Phys. Chem. C* **2012**, *116*, 24695.

21. Gimzewski, J. K.; Joachim, C.; Schlittler, R. R.; Langlais, V.; Tang, H.; Johannsen, I. *Science* **1998**, *281*, 531.

22. Eichberger, M.; Marschall, M.; Reichert, J.; Weber-Bargioni, A.; Auwärter, W.; Wang, R. L. C.; Kreuzer, H. J.; Pennec, Y.; Schiffrin, A.; Barth, J. V. *Nano Lett.* **2008**, *8*, 4608.

23. Lawton, T. J.; Carrasco, J.; Baber, A. E.; Michaelides, A.; Sykes, E. C. H. *Phys. Rev. Lett.* **2011**, *107*, 256101.

24. Horcas, I.; Fernández, R.; Gómez-Rodríguez, J. M.; Colchero, J.; Gómez-Herrero, J.; Baro, A. M. *Rev. Sci. Instrum.* **2007**, *78*, 013705.

25. Aradi, B.; Hourahine, B.; Frauenheim, T. *J. Phys. Chem. A* **2007**, *111*, 5678.

26. Bahn, S. R.; Jacobsen, K. W. *Comput. Sci. Eng.* **2002**, *4*, 56.

27. Koskinen, P.; Mäkinen, V. *Comput. Mater. Sci.* **2009**, *47*, 237.

28. Mäkinen, V.; Koskinen, P.; Häkkinen, H. *Eur. Phys. J. D* **2013**, *67*, 1.

29. Tkatchenko, A.; Scheffler, M. *Phys. Rev. Lett.* **2009**, *102*, 073005.

30. Ruiz, V. G.; Liu, W.; Zojer, E.; Scheffler, M.; Tkatchenko, A. *Phys. Rev. Lett.* **2012**, *108*, 146103.